Hindawi Publishing Corporation
Journal of Nanomaterials
Volume 2015, Article ID 921903, 9 pages
http://dx.doi.org/10.1155/2015/921903

Research Article

Efficiency Enhanced Colloidal Mn-Doped Type II Core/Shell ZnSe/CdS Quantum Dot Sensitized Hybrid Solar Cells

A. Jamshidi,[1] C. Yuan,[1] V. Chmyrov,[2] J. Widengren,[2] L. Sun,[3] and H. Ågren[1]

[1]*Department of Theoretical Chemistry and Biology, School of Biotechnology, Royal Institute of Technology (KTH), 106 91 Stockholm, Sweden*
[2]*Department of Applied Physics/Bimolecular Physics, School of Science, Royal Institute of Technology (KTH), 106 91 Stockholm, Sweden*
[3]*Organic Chemistry, Centre of Molecular Devices, Department of Chemistry, School of Chemical Science and Engineering, Royal Institute of Technology (KTH), 100 44 Stockholm, Sweden*

Correspondence should be addressed to A. Jamshidi; jamshidl@kth.se

Received 15 June 2015; Revised 16 July 2015; Accepted 2 August 2015

Academic Editor: Jun Chen

Colloidal Mn-doped ZnSe/CdS core/shell quantum dots (QDs) are synthesized for the first time and employed as a strategy to boost the power conversion efficiency of quantum dot sensitized solar cells. By using Mn-doping as a band gap engineering tool for core/shell QDs an effective improvement of absorption spectra could be obtained. The mid-states generated by a proper Mn content alleviate carrier separation and enhance the electron injection rate, thus facilitating electron transport to the TiO_2 substrate. It is demonstrated that a device constructed with 0.25% Mn-doped ZnSe/CdS leads to an enhancement of the electron injection rate and power conversion efficiency by 4 times and 1.3, respectively.

1. Introduction

Nanotechnology has led to huge progress in the use of semiconductor nanocrystals for applications in diverse areas like organic light emitting diodes [1], biosensing, biolabeling [2, 3], solar cells [4–6], and imaging and detection [7], to mention a few examples. The world energy demands for renewable and cheap resources of solar energy have generated a large interest in sensitized solar cell technology due to high power conversion efficiency with low cost of production [8, 9]. Among various kinds of sensitizers employed in sensitized solar cells, quantum dots (QDs) are regarded as promising candidates by virtue of their size-dependent optical and electronic properties, high light-absorption ability, photostability, and multiple exciton generation [10]. In particular, type II core/shell quantum dots are promising for efficient sensitization due to their long-time charge separation and possibility for electron confinement in the conduction band of the shell when their band structure is carefully designed [7, 11]. These nanoscale crystals are capable of integrating multistructures with different functionalization into a single nanoscale particle with controllable electronic structure for development of photovoltaic cells. In this heterostructure, the core and shell are made up of two different semiconductors, with a higher conduction (valence) band of the core than the conduction (valence) band of the shell (Scheme 1).

This offers charge carrier localization in two separate materials so that electrons and holes are confined in the shell and core, respectively. Moreover, the use of type II nanocrystals in solar cell applications leads to better power conversion efficiency compared to the corresponding nanocrystals made up entirely from the core or shell materials [12, 13]. Apart from the wide photon absorption range for type II QDs, the improvement also refers to an effective charge separation of electron-hole pairs in the type II nanostructures that facilitates electron abstraction from QDs, suppresses recombination, and therefore leads to better electron transportation [14–16]. It follows that much recent research efforts have been devoted to the synthesis of different type II core/shell structured QDs, like TiO_2/CdS [17], CdSe/ZnSe [18], CdTe/CdSe [19–22], CdTe/CdS [23], CdSe/ZnTe [24], CdSe/ZnTe [25], ZnTe/CdSe [26, 27], CdS/CdSe [28], CdS/ZnSe [16, 18], and

ZnSe/CdS [29], as well as to the use of such QDs in emerging technology for solar cell applications. As an example, theoretical calculations from density-functional and many-body perturbation theory show the conduction and valence band offsets of 0.66 and 0.32 eV for ZnSe/CdS, respectively [30]. Since the effective mass of the electron is lower than the hole in ZnSe [31, 32], one can expect efficient conductivity in the ZnSe/CdS interface particularly where the electron accumulation is made by doping a paramagnetic material like Mn with semifilled d orbital.

It has been shown that use of CdTe/CdSe core/shell nanocrystals prepared by the one-pot synthesis method without core seed purification could make structural and optical properties of nanocrystals comparable to the nanocrystals synthesized using purified core seed, which can give higher absorption and better crystallinity [33]. Neo et al. have investigated the effect of shell thickness and surface passivation as another strategy to improve the efficiency of type II PbS/CdS-based solar cells [34]. Metal ion doping as a band gap engineering tool has also been employed for improvement of type II-based solar cell performance because metal ions could make changes in the Fermi level, band gap, and conductance [35]. Particularly, Mn-doping was recently used in CdS/CdSe sensitized cells as a strategy to boost solar cell efficiency due to very long lifetime of Mn d–d transitions ($^4T_1$-$^6A_1$) [36]. Mn-doping in semiconductors like ZnS, ZnSe, CdS, and CdSe shows dramatic increase in lifetime due to the spin forbidden $^4T_1$-$^6A_1$ transition of the Mn [37–42]. In case of Mn-doped CdS, through doping with Mn^{2+}, a pair of d bands ($^4T_1$ and $^6A_1$) is inserted between the conduction and valence bands of CdS QDs, which alters the electron-hole separation and recombination dynamics, allowing the generation of long-lived charge carriers with microsecond-scale lifetime more slowly than in the case of undoped QDs [37]. Utilization and transfer (transfer of electron and hole toward TiO_2 substrate and electrolyte, resp.) of these long-lived and special-separated carriers by band alignment engineering in core/shell structures should be a superior opportunity to design a QDSSCs device with higher power conversion efficiency. To the best of our knowledge, Mn-doped ZnSe/CdS has not been synthesized and investigated in quantum dots sensitized solar cells (QDSSCs). Since the lattice constant of the CdS shell is larger than that of the ZnSe core (5.82 Å and 5.67 Å for shell and core, resp.), CdS will become strained if it is carefully grown on ZnSe with a smaller lattice constant. In case of strain, both the direct and indirect band gaps (Γ- and L-band, resp.) in the CdS shell are affected by the strain amount and type (compressive or tensile). As the direct band gap shrinks faster than the indirect one in a strained material, *n*-type doping like Mn^{2+}-doping could make Γ-band transitions suitable for detecting the light [43–45].

Here we present a colloidal synthesis of a novel type II Mn-doped ZnSe/CdS core/shell QD system as sensitizer with different Mn concentration (0–3%) and test its utilization in QD sensitized solar cells. This is the first time that Mn-doped ZnSe/CdS core/shell QDs are successfully synthesized by the method of hot injection and used as a strategy to boost solar cell efficiency. As explained in what is to follow it was found that a proper balance of Mn concentration could tailor the band gap and core/shell conduction band edge, causing a better electron transfer from QDs to the TiO_2 photoelectrode, a broader absorption, and, consequently, higher solar cell efficiency.

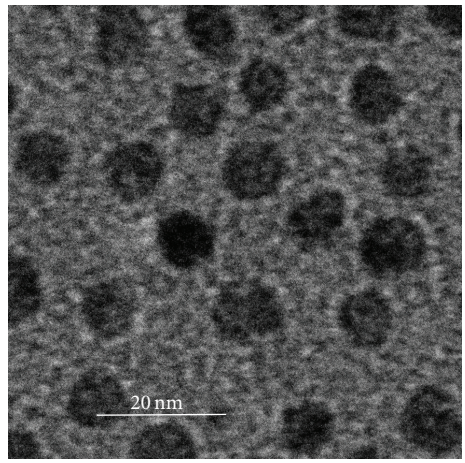

Figure 1: TEM image of colloidal ZnSe/CdS core/shell.

2. Results and Discussions

Novel Mn-doped ZnSe/CdS QDs with different Mn concentration were synthesized by hot injection method. To investigate the effect of doping, all QDs were synthesized at the same conditions and with the same amount of ZnSe cores. To get precise amount of ZnSe core, they were synthesized in one batch and after washing by methanol and acetone, they were divided into several parts to be utilized as ZnSe core in ZnSe/CdS and Mn-doped ZnSe/CdS. To grow shell material onto ZnSe core, the mixture of S and (Mn-doped) Cd precursors was slowly injected into core solution at 240°C, followed by keeping 240°C for 20 min. Afterwards the reaction was cooled down to room temperature for purification and characterization. Transmission electron microscopy, operating in 100 KV, was employed to evaluate quality and size distribution of the nanocrystals. TEM images of ZnSe/CdS core/shell (Figure 1) demonstrate the size of core/shell to be 6-7 nm.

In order to measure the actual Mn concentration incorporated into the nanocrystals, inductively coupled plasma atomic emission spectroscopy (ICP-AES, Thermo Scientific ICAP 6500) was employed. Nanocrystals were digested completely with nitric acid (67%, 0.1 mM) and diluted with DI water to obtain 10 mL of clear solution for ICP-AES measurement [46–48]. The results with details are listed in Table 1 where the real Mn/Cd molar ratio is confirmed.

After being successful in synthesizing the QDs, we prepared different photoanodes sensitized with these QDs: (A) ZnSe, (B) pure ZnSe/CdS and doped ZnSe/CdS with different concentration of Mn: (C) 0.25, (D) 0.5, (E) 1,

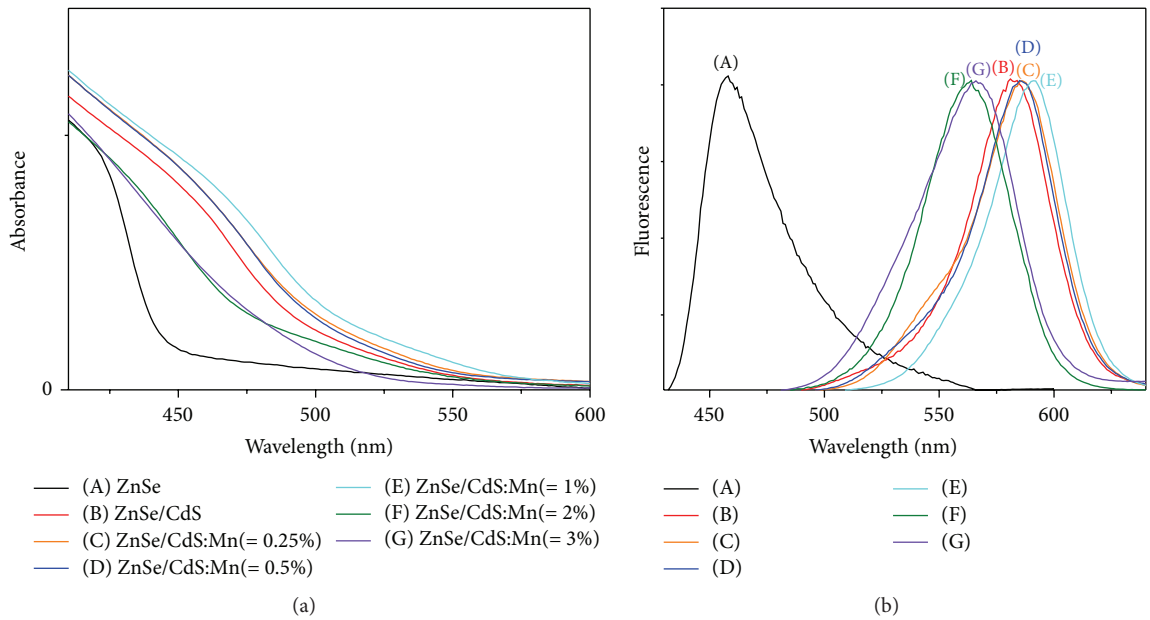

Figure 2: Absorption of QDs-deposited photoelectrodes and photoluminescence of QDs: (A) ZnSe core, (B) pure ZnSe/CdS core/shell and Mn-doped ZnSe/CdS with concentration of (C) 0.25, (D) 0.5, (E) 1, (F) 2, and (G) 3%.

Table 1: Summary of Cd and Mn concentration of nanocrystals.

Samples	(C)	(D)	(E)	(F)	(G)
Mn2576 (ppm)	554	582	523	545	564
Mn2576 (ppm)	0.7423	1.383	2.5000	2.2060	7.9190
Cd (mmol/L)	4.9283	4.2878	4.6526	4.8483	5.0173
Mn (mmol/L)	0.0135	0.0251	0.0455	0.0947	0.1441
Real Mn/Cd (%)	0.2739	0.5853	0.9779	1.9532	2.8720
Expected Mn/Cd (%)	0.25	0.5	1	2	3

(F) 2, and (G) 3%. Figure 2 shows the absorption of QDs-deposited photoelectrodes and fluorescence of QDs dispersed in chloroform. It was seen that pure ZnSe/CdS give broader absorption with a band edge up to 488 nm compared to ZnSe with 437 nm. It shows that both the absorption and emission peak wavelengths in type II ZnSe/CdS core/shell QDs are much longer than those of the pure core or shell materials, resulting from the fact that the energy states (conduction and valence band) for the photogenerated electrons and holes are located in CdS shell and ZnSe core, respectively.

In order to calculate the band gap of the nanocrystals, the absorption coefficient (α) was applied for near-edge optical absorption using the following equation [49, 50]:

$$\alpha h\nu = k\left(h\nu - E_g\right)^{1/2}, \quad (1)$$

where k is a constant and E_g is the optical band gap. According to the graph in Figure 3 plotted for $(\alpha h\nu)^2$ in terms of $(h\nu)$, the band gap E_g values of the nanocrystals were obtained from extrapolating the straight portion of the curve to zero absorption coefficients and they are listed in Table 2.

Therefore, the heterostructure band gap corresponds to the energy separation between the conduction band (CB)

Table 2: Band gap values of nanocrystals derived from Figure 3.

Samples	(A)	(B)	(C)	(D)	(E)	(F)	(G)
Optical band gap (eV)	2.81	2.52	2.48	2.49	2.44	2.61	2.59
Absorption band edge (nm)	437	488	495	493	504	471	474

edge of the shell and the valence band (VB) edge of the core [11, 16], which results in a smaller band gap and a broader absorption spectrum compared to the ZnSe or CdS nanocrystals. Although there is a red shift for low concentration of Mn (0.25–1%), a blue shift is obtained for high concentration (2-3%). The red and blue shifts are attributed to the decrease and increase of the band gap (Table 2), respectively. The band gap decreased for these samples of (C)–(E) and increased for these samples of (F)-(G) due to the contribution of Mn as a metal dopant in CdS and the low solid solubility of Mn (<1%) in the CdS nanocrystals [51–54]. It means that, below 1%, introduction of Mn could lead to decrease of the band gap but, after 1%, it leads to increase of the band gap because of the MnS phase.

To examine the performance of the devices, they were tested under AM 1.5 G simulated solar irradiation with intensity of 100 mW·cm^{-2}. Figure 4 shows the J-V characteristics of solar cell devices sensitized with various QDs. The device parameters including the short-circuit current (J_{SC}), open-circuit voltage (V_{OC}), fill factor (ff), and power conversion efficiency (η) of all samples are summarized in Table 3.

The ZnSe/CdS core/shell shows much higher current than the ZnSe core which may be attributed to special carrier extraction and extension of the light-absorption range in type II heterostructures. Compared to previous work in which the CdS shell of the investigated ZnSe/CdS QDs was synthesized by deposition of Cd and S separately [11], in this study the

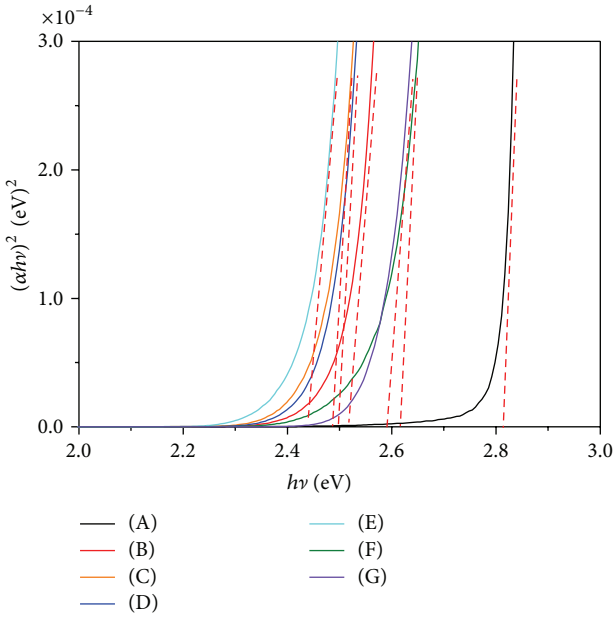

Figure 3: Plot of $(\alpha h\nu)^2$ versus $h\nu$ for different QDs.

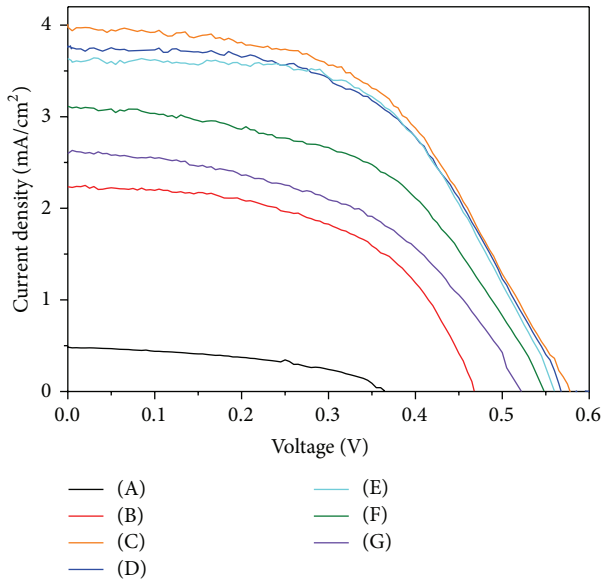

Figure 4: Current-voltage characteristics of the QDSSCs device sensitized with various nanocrystals: (A) ZnSe core, (B) pure ZnSe/CdS core/shell and Mn-doped ZnSe/CdS with concentration of (C) 0.25, (D) 0.5, (E) 1, (F) 2, and (G) 3%.

colloidal ZnSe/CdS core/shell, of which the CdS shell was synthesized by direct deposition of mixture of Cd and S solution, shows higher current and voltage and more than 2 times higher efficiency of 0.47 V and 2.23 mA and 0.56%, respectively, indicating the better crystallization quality of CdS shell synthesized by direct deposition. The strain is another issue in heterostructures that can increase electron mobility [55, 56]. Since the crystal size of CdS bulk (5.82) is bigger than the ZnSe bulk (5.67 Å) [57], one can expect strain

Table 3: Summary of device parameters.

Samples	(A)	(B)	(C)	(D)	(E)	(F)	(G)
V_{oc} (V)	0.365	0.470	0.580	0.575	0.545	0.535	0.508
J_{sc} (mA/cm^2)	0.484	2.235	4.011	3.753	3.634	3.109	2.594
ff	0.852	0.537	0.549	0.553	0.595	0.524	0.513
η (%)	0.15	0.565	1.276	1.194	1.179	0.871	0.674

in the CdS crystals. Since the strain can lead to enhanced electron transport as reported, for instance, in [58], it can be expected that the electrons in the strained CdS shell are transported faster than in unstrained CdS.

A device sensitized with low Mn-doped ZnSe/CdS (0.25%) shows a dramatic increase in all device parameters with about 10 times and 3 times higher efficiency compared to ZnSe and ZnSe/CdS, respectively. Since all samples are coated with 2 cycles of a ZnS SILAR layer, which blocks the electron recombination with the electrolyte [59] and passivates defect states that can trap electron-hole pairs [60], we expect a stabilizing effect by this coating. In case of the Mn-doped ZnSe/CdS sensitized device, the open-circuit voltage, short-circuit current, fill factor, and consequently device efficiency decrease with increase of Mn concentration due to the decrease of absorption range and the increase in nanocrystal band gap (Figures 2 and 3). New energy states in the band gap of the nanocrystal can make the carriers better separated and decrease recombination [12–14].

The best values of device parameters are found for the lowest Mn concentration, possibly due to lower carrier recombination induced by new states generated by proper concentrations of Mn. It should also be mentioned that, like Mn-doped GaAs [61], Mn atoms can occupy three types of sites in the Cd_{1-2x} Mn_x S_x lattice matrix. They can occupy the substitutional or interstitial Cd lattice sites to form Cd_{1-2x} Mn_x S with the wurtzite lattice structure. Mn atoms can also precipitate out to form different phases, for example, MnS nanocrystals. Since the solid solubility of Mn in CdS is too low [51–53] (<1%), less than 1% induces substitutional or interstitial sites and more than 1% induces other phases like MnS that can act as impurity and therefore decrease the device performance.

The Incident Photon to Current Efficiency (IPCE) of all devices was measured to evaluate the photocurrent response to incident light (shown in Figure 5). IPCE, sometimes referred to as external quantum efficiency (EQE), is expressed by the following equation [62]:

$$\mathrm{IPCE}(\lambda) = \mathrm{LHE}(\lambda)\,\eta_{\mathrm{coll}}\phi_{\mathrm{inj}}, \tag{2}$$

where ϕ_{inj} is the quantum yield, η_{coll} is the electron collection efficiency, and LHE(λ) is the light harvesting efficiency at the wavelength λ of the incident light and is derived via

$$\mathrm{LHE}(\lambda) = 1 - 10^{-\mathrm{Abs}(\lambda)}. \tag{3}$$

The power conversion efficiency is comparatively low for devices sensitized by ZnSe due to limited light absorption but increases in ZnSe/CdS. This is related to the broader absorption and the special carrier separation in this type II

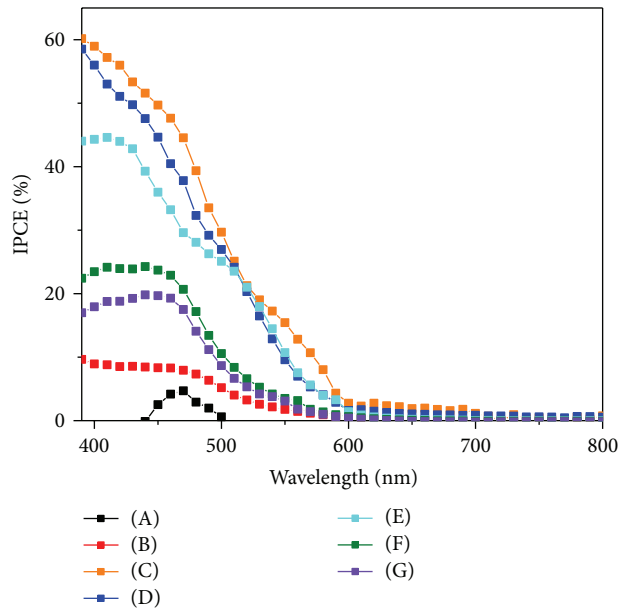

FIGURE 5: The IPCE spectra of devices based on (A) ZnSe, (B) pure ZnSe/CdS and Mn-doped ZnSe/CdS with Mn concentration of (C) 0.25, (D) 0.5, (E) 1, (F) 2, and (G) 3%.

heterostructure. The observed rather dramatic increase in IPCE spectra of Mn-doped ZnSe/CdS compared to undoped ZnSe/CdS may be due to a more efficient electron collection and electron injection efficiency. It is worthwhile to stress that band structure and CB manipulation via band gap engineering (Figures 2 and 3) by proper Mn concentration doped into the nanocrystals not only give superior ability to enhance light absorption but also can facilitate carrier transfer, which may be responsible for the improvement of the device efficiency. However, higher doping ratios may generate impurities or defects like MnS, which can increase charge recombination and inhibit electron injection into the TiO_2 substrate.

The excited states dynamics of QDs were further investigated by time-resolved fluorescence lifetime measurements (experimental details in the supporting information in Supplementary Material available online at http://dx.doi.org/10.1155/2015/921903). Figures 6(a) and 6(b) show the fluorescence emission decay of different QDs deposited on insulator glass and conductive glass/TiO_2, respectively. The fluorescence intensity decay curves recorded from QDs were successfully fitted to a three-exponential decay model. The fitting parameters are summarized in Table S1 (supporting information). The average lifetime of QDs was estimated based on [63]

$$\langle \tau \rangle = \frac{\sum_n \left(a_n \tau_n^2\right)}{\sum_n \left(a_n \tau_n\right)}, \tag{4}$$

where n is the nth exponential component. In our procedure, a triexponential decay model ($n = 3$) was found to be necessary to properly fit the experimental fluorescence decay curves [64, 65], and no substantial improvement in the goodness-of-fit was obtained for higher n. (See fitting residuals in Figures S1 and S2 in the supporting information.)

It is found that the average fluorescence lifetime of ZnSe/CdS QDs (49 ns) is much longer than that of ZnSe (2 ns) when they are attached to the insulator. This is due to special charge separation in type II nanostructures that can decrease their wave function overlap and delay radiative recombination, resulting in a long fluorescence lifetime [11]. It was mentioned that photogenerated holes can be moved to the valence band of ZnSe and that photogenerated electrons will be localized in CdS. When the QDs are attached to the insulator, there is no electron injection, but if deposited to the TiO_2, another electron deactivation route is created that causes electrons to be injected from the QDs into the TiO_2 with lower conduction band energy, which results in a decrease of the lifetime. The corresponding electron injection rate constant can be estimated from [64, 65]

$$K_{et} = \frac{1}{\tau_{(\mathrm{QD+TiO_2})}} - \frac{1}{\tau_{(\mathrm{QD})}}, \tag{5}$$

where $\tau_{(\mathrm{QD})}$ and $\tau_{(\mathrm{QD+TiO_2})}$ are the fluorescence lifetimes of the QDs attached to the TiO_2 and insulator glass, respectively. As it is shown in Table S1, a higher injection rate constant of the QDs is ascribed to the lower Mn-doped type II ZnSe/CdS QDs that are responsible for the efficiency of the device.

To get more understanding of the charge transport in type II ZnSe/CdS QDs with different Mn concentration, a physical model like Scheme 1 is considered. The ZnSe as core is covered by the CdS shell and the conduction bands and valence bands edge of TiO_2, ZnSe core, and CdS shell are formed while considering the quantum confinement effect in the type II heterostructure. Coupling of the ZnSe and CdS moieties leads to special carrier separation and interfacial wave function interaction increased by increasing the Mn concentration. The results indicate that by increasing Mn content until 1% not only is the band gap decreased, which results in special indirect band gap with some red shift of the absorption band edge, but also the device parameters are increased because of lower recombination and enhancement of the electron injection rate. It is notable that the Mn $^4T_1$ mid-state between CdS CB and TiO_2 CB can facilitate electron transfer from QDs into TiO_2. Further amount of doping can reverse the results (not shown here).

3. Conclusions

Novel colloidal Mn-doped ZnSe/CdS core/shell QDs with various Mn concentrations were successfully synthesized and applied to sensitized solar cells. It was demonstrated that QDs with proper Mn-doping could cause an increase in the absorption spectra and red shift in the absorption band edge and in the photoluminescence emission peak. The mid-states generated by Mn can facilitate electron transfer from the QDs to the TiO_2 substrate. With superior light absorption, better carrier separation, and efficient electron injection rate a power conversion efficiency of 1.27% is presented, which is about 2 and 3 times larger than those of core and undoped QDs sensitized solar cells, respectively. The

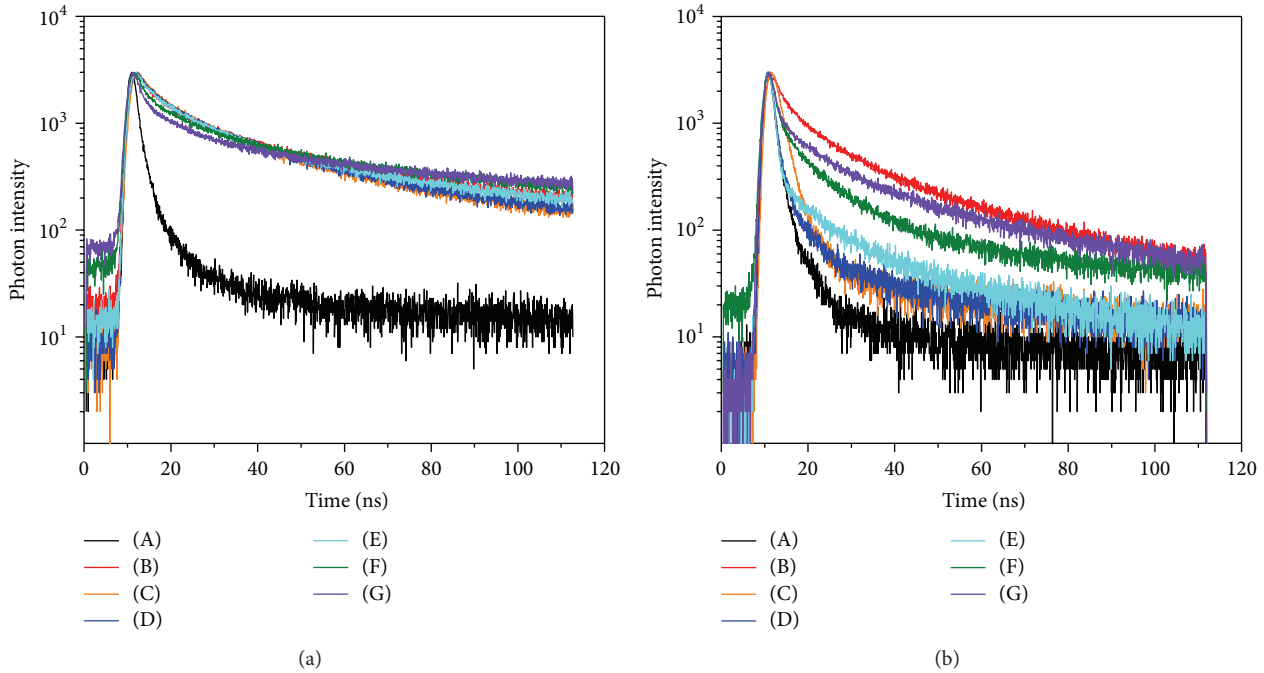

FIGURE 6: Time-resolved fluorescence intensity decay curves of QDs onto (a) insulator and (b) TiO_2 film; QDs: (A) ZnSe, (B) pure ZnSe/CdS and Mn-doped ZnSe/CdS QDs with Mn concentration of (C) 0.25, (D) 0.5, (E) 1, (F) 2, and (G) 3%.

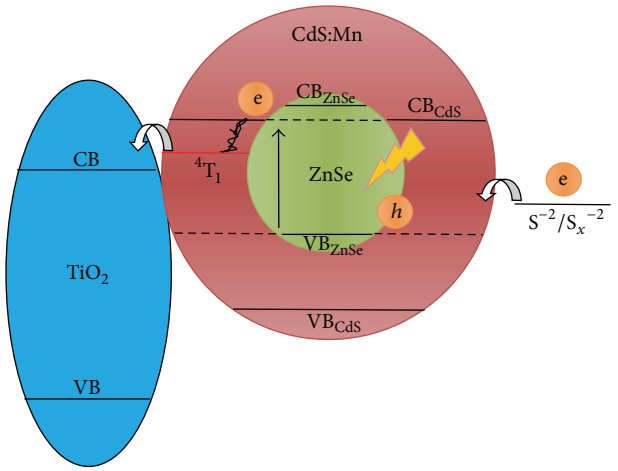

SCHEME 1: Schematic illustration of charge transfer mechanism in Mn-doped ZnSe/CdS.

present work suggests that band structure manipulation in type II core/shell nanostructure offers an effective way to improve light harvesting and control of charge transfer via efficient charge separation in sensitized solar cells and that Mn-doping opens a new window to increase device efficiency. There is a multitude of lines of research to embark upon for future improvement of QDs sensitized solar cell of the kind proposed here. One such line of research concerns surface passivation. In fact, the organic ligands used can act as dangling bonds on the QDs surface and trap carriers, which calls for surface passivation of the QDs as a way to improve device performance, for instance, by using hydrophilic materials or ions. These and other measures will be pursued in our future studies.

4. Experimental

4.1. Quantum Dots Synthesis. Zinc stearate, gray selenium, cadmium oxide, sulfide, and manganese nitrate tetrahydrate were bought from Aldrich Company as precursors for Zn, Se, Cd, S, and Mn sources, respectively. The targeted heteronanocrystals are fabricated by a two-step synthesis composed of the fabrication of ZnSe core nanoparticle followed by a deposition of pure or Mn-doped CdS shell. Synthesis of both ZnSe core and pure or Mn-doped ZnSe/CdS core/shell under different Mn concentrations is based on previously published procedures [16, 29] with some modifications briefly explained as follows.

Firstly, in order to synthesize ZnSe core nanocrystals from organic solution, specific amounts of selenium 0.0118 g and 0.4 mL of trioctylphosphine (TOP) were placed in a one-necked flask while stirring to make selenium dissolved in TOP. The reaction was conducted under nitrogen atmosphere. When the mixture became clear, the solution was kept in a clean syringe to be used in the next step. 0.0950 g zinc stearate, 0.1874 g stearic acid, and 2 mL of octadecane (ODA) were mixed together in a 25 mL three-necked flask. The mixture was slowly heated to 120°C (about 2°C/min) while stirring and pumping to remove additional elements from solution. The mixture was then heated to 240°C under nitrogen flow to make zinc dissolved in ODE where the solution appeared colorless and clear. Then a selenium stock solution prepared in the last step was swiftly injected into

the reaction flask. The solution temperature was controlled and monitored to be kept at about 280°C. After 20 min, the reaction solution was cooled down to 60°C and 5 mL of chloroform was added to the solution to allow the quantum dots to be dissolved and suspended. The product of this step was ZnSe core, which contains byproducts and free ligands. To purify, it was washed 4 times by acetone and methanol. Typically, 5 mL of chloroform, 10 mL of acetone, and 2 mL of methanol were slowly added to the QDs solution followed by centrifugation for 3 min at 12400 rpm. The upper colorless layer was removed and QDs precipitated on the bottom were dissolved in chloroform for the next washing. Monodisperse ZnSe core produced in this step was sealed and kept in a cool and dark area to be used for shell deposition.

For preparing the CdS shell, three steps were considered. First, totally 0.0050 g of sulfur was dissolved in 3 mL of ODE while pumping and heating slowly to 80°C and then cooled to room temperature. Second, totally 0.0190 g of cadmium oxide (in case of Mn-doping, a proper amount of Mn was added to Cd precursor) was mixed in 0.4 mL of oleic acid (OA) and 3.5 mL of ODE in a 25 mL flask while stirring and heating slowly to 100°C. After degassing process, the temperature was increased to 280°C to make Cd dissolved completely in the solution. When the solution became clear, it was cooled down to 60°C. Third, mix these two precursor solutions (S and Cd) together as a source for shell growth. The final mixture was slowly injected (3 mL/h) into the reaction vessel, which contained 375 g ODA and ZnSe core dispersed in 2 mL of ODE at 240°C. After 20 min, the reaction was terminated and cooled down to room temperature for purification by chloroform and acetone.

4.2. Photoanode Preparation. FTO (fluorine tin oxide) conductive glasses (Sigma Aldrich, sheet resistance of 7 Ω/sq) were used as photoelectrode substrates. FTO glasses were cut to targeted size (1 × 2 cm) and sequentially washed by soap, KOH dissolved in 2-propanol, acetone, ethanol, and DI water via sonication for 30 min for each washing step, followed by immersion in 40 mM $TiCl_4$ solution at 80°C for 40 minutes to give a TiO_2 blocking layer. Mesoporous TiO_2 layers were prepared by deposition of three transparent layers and one scattering layer with commercial TiO_2 pastes (Ti-Nanoxide T/SP with 20 nm and Ti-Nanoxide R/SP with > 100 nm particle size for transparent and scattering layer, resp.) by screen-printing technique concluding by heating at 70°C for each layer deposition. The samples were postannealed at 500°C for 30 min to make the layers porous by removing the organic part at high temperature.

QDs dissolved in chloroform were deposited drop by drop on TiO_2 films and left to be dried in the air. Excess QDs not adsorbed on TiO_2 were washed by chloroform. To passivate QDs, ZnS block layers were deposited by two cycles of SILAR method. Each cycle contains dipping the samples into sulfur solution (Na_2S dissolved in DI) for 1 min followed by washing with DI water and zinc solution (zinc nitrate hydrate dissolved in DI) for 1 min followed by washing with DI water.

4.3. Counter Electrode Preparation. Cu_2S counter electrode was prepared by dipping brass sheet (Sigma Aldrich, resistivity of 1.673 μΩ·cm) in hydrochloric acid at 80°C for 10 minutes and then washing with DI water and methanol.

4.4. Device Assembly. Both photoelectrode and Cu_2S counter electrode prepared in the last steps were stocked together by cell spacer while the electrodes were heating at 80°C. The S^{2-}/S_x^{2-} electrolyte (2 M S, 2 M Na_2S, and 0.2 M KCl in a methanol-water (v/v, 3/7) solution) was finally injected into the cell through the hole preconstructed on top of the brass sheet. After electrolyte injection, the hole was sealed by sealing tape for the next electrical characterization.

4.5. Fluorescence Lifetime Measurements by Time-Correlated Single-Photon Counting. Time-correlated single-photon (TCSPC) measurements were performed on a spectrofluorometer with a TCSPC option (FluoroMax3, Horiba Jobin Yvon). A NanoLED (Horiba Jobin Yvon) emitting at 488 nm with a repetition rate of 1 MHz and pulse width of 1,4 ns was used as an excitation. Measurements were stopped when 3000 photon counts were collected in the peak channel using 2048 channels with 0,4 ns/channel. The instrument response function was recorded using a 2% Ludox (Sigma Aldrich) solution. To avoid reabsorption and reemission effects and also not to saturate the detectors, the sample concentration was kept strictly below 5 μM. Recorded curves were fitted with a three-exponential decay using the software Decay Analysis Software v.6 (IHB).

Conflict of Interests

The authors declare that there is no conflict of interests regarding the publication of this paper.

Acknowledgments

The authors acknowledge Jing Huang for helpful advice. This work was supported by a grant from the Swedish Science Research Council (Contract G21-2012-3347).

References

[1] P. O. Anikeeva, J. E. Halpert, M. G. Bawendi, and V. Bulović, "Quantum dot light-emitting devices with electroluminescence tunable over the entire visible spectrum," *Nano Letters*, vol. 9, no. 7, pp. 2532–2536, 2009.

[2] H. Lee, S. W. Yoon, E. J. Kim, and J. Park, "In-situ growth of copper sulfide nanocrystals on multiwalled carbon nanotubes and their application as novel solar cell and amperometric glucose sensor materials," *Nano Letters*, vol. 7, no. 3, pp. 778–784, 2007.

[3] K.-T. Yong, I. Roy, H. Ding, E. J. Bergey, and P. N. Prasad, "Biocompatible near-infrared quantum dots as ultrasensitive probes for long-term in vivo imaging applications," *Small*, vol. 5, no. 17, pp. 1997–2004, 2009.

[4] C. Dong, X. Li, and J. Qi, "First-principles investigation on electronic properties of quantum dot-sensitized solar cells based on anatase TiO_2 nanotubes," *Journal of Physical Chemistry C*, vol. 115, no. 41, pp. 20307–20315, 2011.

[5] F. C. Krebs, S. A. Gevorgyan, and J. Alstrup, "A roll-to-roll process to flexible polymer solar cells: model studies, manufacture and operational stability studies," *Journal of Materials Chemistry*, vol. 19, no. 30, pp. 5442–5451, 2009.

[6] M. Helgesen, R. Søndergaard, and F. C. Krebs, "Advanced materials and processes for polymer solar cell devices," *Journal of Materials Chemistry*, vol. 20, no. 1, pp. 36–60, 2010.

[7] A. M. Smith and S. Nie, "Semiconductor nanocrystals: structure, properties, and band gap engineering," *Accounts of Chemical Research*, vol. 43, no. 2, pp. 190–200, 2010.

[8] B. O'Regan and M. Grätzel, "A low-cost, high-efficiency solar cell based on dye-sensitized colloidal TiO_2 films," *Nature*, vol. 353, no. 6346, pp. 737–740, 1991.

[9] A. Yella, H.-W. Lee, H. N. Tsao, C. Yi, A. K. Chandiran, and M. K. Nazeeruddin, "Porphyrin-sensitized solar cells with cobalt (II/III)-based redox electrolyte exceed 12 percent efficiency," *Science*, vol. 334, no. 6056, pp. 629–634, 2011.

[10] L.-H. Lai, L. Protesescu, M. V. Kovalenko, and M. A. Loi, "Sensitized solar cells with colloidal PbS-CdS core-shell quantum dots," *Physical Chemistry Chemical Physics*, vol. 16, no. 2, pp. 736–742, 2014.

[11] Z. Ning, H. Tian, C. Yuan et al., "Solar cells sensitized with type-II ZnSe-CdS core/shell colloidal quantum dots," *Chemical Communications*, vol. 47, no. 5, pp. 1536–1538, 2011.

[12] X.-Y. Yu, B.-X. Lei, D.-B. Kuang, and C.-Y. Su, "Highly efficient CdTe/CdS quantum dot sensitized solar cells fabricated by a one-step linker assisted chemical bath deposition," *Chemical Science*, vol. 2, no. 7, pp. 1396–1400, 2011.

[13] S. Itzhakov, H. Shen, S. Buhbut, H. Lin, and D. Oron, "Type-II quantum-dot-sensitized solar cell spanning the visible and near-infrared spectrum," *Journal of Physical Chemistry C*, vol. 117, no. 43, pp. 22203–22210, 2013.

[14] L. P. Balet, S. A. Ivanov, A. Piryatinski, M. Achermann, and V. I. Klimov, "Inverted core/shell nanocrystals continuously tunable between type-I and type-II localization regimes," *Nano Letters*, vol. 4, no. 8, pp. 1485–1488, 2004.

[15] H. Wang, T. Wang, X. Wang et al., "Double-shelled ZnO/CdSe/CdTe nanocable arrays for photovoltaic applications: microstructure evolution and interfacial energy alignment," *Journal of Materials Chemistry*, vol. 22, no. 25, pp. 12532–12537, 2012.

[16] S. A. Ivanov, A. Piryatinski, J. Nanda et al., "Type-II core/shell CdS/ZnSe nanocrystals: synthesis, electronic structures, and spectroscopic properties," *Journal of the American Chemical Society*, vol. 129, no. 38, pp. 11708–11719, 2007.

[17] C. Cao, C. Hu, W. Shen, S. Wang, Y. Tian, and X. Wang, "Synthesis and characterization of TiO_2/CdS core-shell nanorod arrays and their photoelectrochemical property," *Journal of Alloys and Compounds*, vol. 523, pp. 139–145, 2012.

[18] M. Danek, K. F. Jensen, C. B. Murray, and M. G. Bawendi, "Synthesis of luminescent thin-film CdSe/ZnSe quantum dot composites using CdSe quantum dots passivated with an overlayer of ZnSe," *Chemistry of Materials*, vol. 8, no. 1, pp. 173–180, 1996.

[19] S. Taniguchi, M. Green, S. B. Rizvi, and A. Seifalian, "The one-pot synthesis of core/shell/shell CdTe/CdSe/ZnSe quantum dots in aqueous media for in vivo deep tissue imaging," *Journal of Materials Chemistry*, vol. 21, no. 9, pp. 2877–2882, 2011.

[20] W. Zhang, G. Chen, J. Wang, B.-C. Ye, and X. Zhong, "Design and synthesis of highly luminescent near-infrared-emitting water-soluble CdTe/CdSe/ZnS Core/Shell/Shell quantum dots," *Inorganic Chemistry*, vol. 48, no. 20, pp. 9723–9731, 2009.

[21] S. Kim, B. Fisher, H.-J. Eisler, and M. Bawendi, "Type-II quantum dots: CdTe/CdSe(core/shell) and CdSe/ZnTe(core/shell) heterostructures," *Journal of the American Chemical Society*, vol. 125, no. 38, pp. 11466–11467, 2003.

[22] J. Wang, I. Mora-Seró, Z. Pan et al., "Core/shell colloidal quantum dot exciplex states for the development of highly efficient quantum-dot-sensitized solar cells," *Journal of the American Chemical Society*, vol. 135, no. 42, pp. 15913–15922, 2013.

[23] O. Schöps, N. Le Thomas, U. Woggon, and M. V. Artemyev, "Recombination dynamics of CdTe/CdS core-shell nanocrystals," *Journal of Physical Chemistry B*, vol. 110, no. 5, pp. 2074–2079, 2006.

[24] M. W. DeGroot, N. J. Taylor, and J. F. Corrigan, "Molecular nanocluster analogues of CdSe/ZnSe and CdTe/ZnTe core/shell nanoparticles," *Journal of Materials Chemistry*, vol. 14, no. 4, pp. 654–660, 2004.

[25] C.-T. Cheng, C.-Y. Chen, C.-W. Lai et al., "Syntheses and photophysical properties of type-II CdSe/ZnTe/ZnS (core/shell/shell) quantum dots," *Journal of Materials Chemistry*, vol. 15, no. 33, pp. 3409–3414, 2005.

[26] R. G. Xie, X. H. Zhong, and T. Basche, "Synthesis, characterization, and spectroscopy of type-II core/shell semiconductor nanocrystals with ZnTe cores," *Advanced Materials*, vol. 17, no. 22, pp. 2741–2745, 2005.

[27] S. Jiao, Q. Shen, I. Mora-Seró et al., "Band engineering in core/shell ZnTe/cdse for photovoltage and efficiency enhancement in exciplex quantum dot sensitized solar cells," *ACS Nano*, vol. 9, no. 1, pp. 908–915, 2015.

[28] Z. Pan, H. Zhang, K. Cheng, Y. Hou, J. Hua, and X. Zhong, "Highly efficient inverted type-I CdS/CdSe core/shell structure QD-sensitized solar cells," *ACS Nano*, vol. 6, no. 5, pp. 3982–3991, 2012.

[29] A. Nemchinov, M. Kirsanova, N. N. Hewa-Kasakarage, and M. Zamkov, "Synthesis and characterization of type II ZnSe/CdS core/shell nanocrystals," *Journal of Physical Chemistry C*, vol. 112, no. 25, pp. 9301–9307, 2008.

[30] Y. Hinuma, A. Grüneis, G. Kresse, and F. Oba, "Band alignment of semiconductors from density-functional theory and many-body perturbation theory," *Physical Review B*, vol. 90, Article ID 155405, 2014.

[31] D. T. F. Marple, "Electron effective mass in ZnSe," *Journal of Applied Physics*, vol. 35, no. 6, pp. 1879–1882, 1964.

[32] H. E. Ruda, "A theoretical analysis of electron transport in ZnSe," *Journal of Applied Physics*, vol. 59, no. 4, pp. 1220–1231, 1986.

[33] P. Patil, C. Laltlanzuala, and S. Datta, "Sensitized solar cell from type-II CdTe/CdSe core/shell nanocrystals synthesized without seed purification at low temperature," *Journal of Alloys and Compounds*, vol. 607, pp. 230–237, 2014.

[34] D. C. J. Neo, C. Cheng, S. D. Stranks et al., "Influence of shell thickness and surface passivation on PbS/CdS Core/Shell colloidal quantum dot solar cells," *Chemistry of Materials*, vol. 26, no. 13, pp. 4004–4013, 2014.

[35] X. Qi, X. Zou, and S. He, "La doping of CdS for enhanced CdS/CdSe quantum dot cosensitized solar cells," *Journal of Chemistry*, vol. 2015, Article ID 710140, 7 pages, 2015.

[36] P. K. Santra and P. V. Kamat, "Mn-doped quantum dot sensitized solar cells: a strategy to boost efficiency over 5%," *Journal of the American Chemical Society*, vol. 134, no. 5, pp. 2508–2511, 2012.

[37] P. Wu, J.-B. Pan, X.-L. Li, X. Hou, J.-J. Xu, and H.-Y. Chen, "Long-lived charge carriers in mn-doped CdS quantum dots for photoelectrochemical cytosensing," *Chemistry—A European Journal*, vol. 21, no. 13, pp. 5129–5135, 2015.

[38] R. Beaulac, P. I. Archer, and D. R. Gamelin, "Luminescence in colloidal Mn^{2+}-doped semiconductor nanocrystals," *Journal of Solid State Chemistry*, vol. 181, no. 7, pp. 1582–1589, 2008.

[39] V. A. Vlaskin, N. Janssen, J. van Rijssel, R. Beaulac, and D. R. Gamelin, "Tunable dual emission in doped semiconductor nanocrystals," *Nano Letters*, vol. 10, no. 9, pp. 3670–3674, 2010.

[40] R. Beaulac, P. I. Archer, X. Liu et al., "Spin-polarizable excitonic luminescence in colloidal Mn^{2+}-doped CdSe quantum dots," *Nano Letters*, vol. 8, no. 4, pp. 1197–1201, 2008.

[41] R. Beaulac, P. I. Archer, J. Van Rijssel, A. Meijerink, and D. R. Gamelin, "Exciton storage by Mn^{2+} in colloidal Mn^{2+}-Doped CdSe quantum dots," *Nano Letters*, vol. 8, no. 9, pp. 2949–2953, 2008.

[42] A. A. Bol and A. Meijerink, "Long-lived Mn^{2+} emission in nanocrystalline ZnS:Mn^{2+}," *Physical Review B—Condensed Matter and Materials Physics*, vol. 58, no. 24, Article ID R15997, 1998.

[43] J. F. Liu, D. D. Cannon, K. Wada et al., "Tensile strained Ge *p-i-n* photodetectors on Si platform for C and L band telecommunications," *Applied Physics Letters*, vol. 87, no. 1, Article ID 011110, 2005.

[44] J. Wang, W. Y. Loh, H. Zang et al., "Integration of tensile-strained Ge p-i-n photodetector on advanced CMOS platform," in *Proceedings of the 4th International Conference on Group IV Photonics (GFP '07)*, pp. 52–54, September 2007.

[45] A. Jamshidi, M. Noroozi, M. Moeen et al., "Growth of GeSnSiC layers for photonic applications," *Surface & Coatings Technology*, vol. 230, pp. 106–110, 2013.

[46] J. Tang, K. W. Kemp, S. Hoogland et al., "Colloidal-quantum-dot photovoltaics using atomic-ligand passivation," *Nature Materials*, vol. 10, no. 10, pp. 765–771, 2011.

[47] F. Gong, H. Wang, X. Xu, G. Zhou, and Z.-S. Wang, "In situ gowth of $Co_{0.85}Se$ and $Ni_{0.85}Se$ on conductive substrates as high-performance counter electrodes for dye-sensitized solar cells," *Journal of the American Chemical Society*, vol. 134, no. 26, pp. 10953–10958, 2012.

[48] C. Steinhagen, T. B. Harvey, C. J. Stolle, J. Harris, and B. A. Korgel, "Pyrite nanocrystal solar cells: promising, or fool's gold?" *Journal of Physical Chemistry Letters*, vol. 3, no. 17, pp. 2352–2356, 2012.

[49] R. Sahraei, G. M. Aval, and A. Goudarzi, "Compositional, structural, and optical study of nanocrystalline ZnS thin films prepared by a new chemical bath deposition route," *Journal of Alloys and Compounds*, vol. 466, no. 1-2, pp. 488–492, 2008.

[50] H. R. Dizaji, A. J. Zavaraki, and M. H. Ehsani, "Effect of thickness on the structural and optical properties of ZnS thin films prepared by flash evaporation technique equipped with modified feeder," *Chalcogenide Letters*, vol. 8, no. 4, pp. 231–237, 2011.

[51] M. Liu, L. Zhang, X. He et al., "L-cystine-assisted hydrothermal synthesis of $Mn_{1-x}Cd_xs$ solid solutions with hexagonal wurtzite structure for efficient photocatalytic hydrogen evolution under visible light irradiation," *Journal of Materials Chemistry A*, vol. 2, no. 13, pp. 4619–4626, 2014.

[52] R. Chauhan, A. Kumar, and R. P. Chaudhary, "Synthesis, structural and photocatalytic studies of Mn-doped CdS nanoparticles," *Research on Chemical Intermediates*, vol. 39, no. 2, pp. 645–657, 2013.

[53] M. Elango, K. Gopalakrishnan, S. Vairam, and M. Thamilselvan, "Structural, optical and magnetic studies on non-aqueous synthesized CdS:Mn nanomaterials," *Journal of Alloys and Compounds*, vol. 538, pp. 48–55, 2012.

[54] H. Zhai, L. Cao, G. Su, W. Liu, and B. Dong, "Synthesis, structural and optical properties of water-soluble Mn-doped CdS nanocrystals," *Micro and Nano Letters*, vol. 6, no. 4, pp. 257–260, 2011.

[55] F. M. Bufler, P. Graf, S. Keith, and B. Meinerzhagen, "Full band Monte Carlo investigation of electron transport in strained Si grown on $Si_{1-x}Ge_x$ substrates," *Applied Physics Letters*, vol. 70, no. 16, pp. 2144–2146, 1997.

[56] P. Dollfus, S. Galdin, and P. Hesto, "Monte-Carlo investigation of in-plane electron transport in tensile strained Si and $Si_{1-Y}C_y$ ($Y \leq 0.03$)," *European Physical Journal-Applied Physics*, vol. 7, no. 1, pp. 73–77, 1999.

[57] T. Ido, "Energy bandgap and lattice constant contours of II–VI quaternary alloys," *Journal of Electronic Materials*, vol. 9, no. 5, pp. 869–882, 1980.

[58] Y. G. Wang, Q. L. Zhang, T. H. Wang, W. Han, and S. X. Zhou, "Improvement of electron transport in a ZnSe nanowire by in situ strain," *Journal of Physics D: Applied Physics*, vol. 44, no. 12, Article ID 125301, 2011.

[59] I. Mora-Seró, S. Giménez, F. Fabregat-Santiago et al., "Recombination in quantum dot sensitized solar cells," *Accounts of Chemical Research*, vol. 42, no. 11, pp. 1848–1857, 2009.

[60] N. Guijarro, J. M. Campiña, Q. Shen, T. Toyoda, T. Lana-Villarreal, and R. Gómez, "Uncovering the role of the ZnS treatment in the performance of quantum dot sensitized solar cells," *Physical Chemistry Chemical Physics*, vol. 13, no. 25, pp. 12024–12032, 2011.

[61] K. M. Yu, W. Walukiewicz, T. Wojtowicz et al., "Effect of the location of Mn sites in ferromagnetic $Ga_{1-x}Mn_xAs$ on its Curie temperature," *Physical Review B*, vol. 65, no. 20, Article ID 201303, 2002.

[62] M. Grätzel, "Solar energy conversion by dye-sensitized photovoltaic cells," *Inorganic Chemistry*, vol. 44, no. 20, pp. 6841–6851, 2005.

[63] D. R. James, Y.-S. Liu, P. De Mayo, and W. R. Ware, "Distributions of fluorescence lifetimes: consequences for the photophysics of molecules adsorbed on surfaces," *Chemical Physics Letters*, vol. 120, no. 4-5, pp. 460–465, 1985.

[64] A. Kongkanand, K. Tvrdy, K. Takechi, M. Kuno, and P. V. Kamat, "Quantum dot solar cells. Tuning photoresponse through size and shape control of CdSe-TiO_2 architecture," *Journal of the American Chemical Society*, vol. 130, no. 12, pp. 4007–4015, 2008.

[65] Z. Ning, H. Tian, H. Qin et al., "Wave-function engineering of CdSE/CdS core/shell quantum dots for enhanced electron transfer to a TiO_2 Substrate," *The Journal of Physical Chemistry C*, vol. 114, no. 35, pp. 15184–15189, 2010.